*Linh Truong-Hong[(1)], and Debra F. Laefer[(2)]**

VALIDATING COMPUTATIONAL MODELS FROM LASER SCANNING DATA FOR HISTORIC FACADES

ABSTRACT: Increasingly, remote sensing is being used as the basis for computational models. With new approaches rapidly emerging, questions arise as to how to validate and assess the resulting models, as they tend to include at least some level of geometric inexactitude. This paper proposes a set of parameters and procedures for evaluating the usefulness of computational models for structural analysis of historic facades subjected to adjacent construction work. To test the usability of such an approach, three brick buildings were scanned with a terrestrial laser scanner. The data were processed with a recently proposed set of algorithms, and the reliability of the resulting solid models was evaluated by comparing finite element results from auto-generated solid models versus those based on measured drawings. The proposed validation process considers overall response, as well as local behavior. The results show the importance of using both conventional values and project specific parameters.

KEYWORDS: remote sensing; terrestrial laser scanning data; finite element analysis; foundation settlement; geometric validation; solid model generation

Introduction

Various forms of remote sensing including laser scanning are being used to document the built environment. This is occurring in transportation assessment [1], disaster planning [2], structural health monitoring [3], and structural analysis [4,5]. Nowhere is this need more acute than for tunneling projects. To evaluate the impact of large-scale, urban infrastructure projects on adjacent buildings, geometric building models are required. For older and/or historic buildings this information is rarely readily available, even in the form of post-construction, measured drawings. Thus, manual surveying and manual Computer-Aided Design (CAD) model generation are commonly undertaken as requisite steps to importing a building's geometry into a Finite Element Method (FEM) program for structural analysis. The approach is expensive and time consuming. Yet, it is often undertaken as part of the preventive measures of multi-million euro tunneling contracts (e.g. [6,7]).

As an alternative to manual surveying, various automated and semi-automated approaches are being developed for remote sensing data (as recently reviewed by Laefer et al. [8]), thereby raising the question of how to evaluate the quality of these resulting solid models, especially in light of known mild geometric inexactitudes. An area where this is rapidly gaining importance is in the use of Light Detection and Ranging (LiDAR) [both airborne laser scanning (ALS) and terrestrial laser scanning (TLS)], as this technology can acquire an object's surface geometry quickly [9]. The newest uses of LiDAR go beyond mere visualization and include even micro-climate modeling [10]. To address this emerging issue, this paper proposes a means to validate and compare the quality of solid models of historic façades generated from remote sensing data.

Related works

In 2006, the American Society of Mechanical Engineers proposed a guide for verification and validation in computational solid mechanics [11]. In that document, the distinction was made between "Verification: the process of determining that a computational model accurately represents the underlying mathematical model and its solution." and "Validation: the process of determining the degree to which a model is an accurate representation of the real world from the perspective of the intended uses of the model." In structural engineering, verification can be done by comparing a solution to a known exact one (e.g. Guenfoud et al. [12]), but many problems do not have a closed-form solution. Thus, validation must be achieved via an experimental model (Type I) or through other numerical simulations (Type II), both of which contain uncertainties. As analyses of unreinforced masonry buildings (UMBs) have no closed-form solutions, validation through experimental and/or numerical means is needed. While mesh sensitivity is tested through convergence (i.e. increasing mesh fineness until no meaningful distinction occurs in a single value output), the main issue of the overall appropriateness of the model remains poorly defined, and specific guidance does not exist regarding the particular challenges of assessing auto-generated meshes from remote sensing data.

(1) PhD, Urban Modelling Group (UMG), School of Civil, Structural, and Environmental Engineering (SCSEE), University College Dublin (UCD), Newstead G67, Belfield, Dublin 4, Ireland. Email: linh.truonghong@gmail.com

(2) Associate Professor and Lead PI, UMG, SCSEE, UCD, Newstead G25, Belfield, Dublin 4, Ireland. Email: debra.laefer@ucd.ie, corresponding author

To date, various parameters singularly or in combination have been proposed to look at overall performance of unreinforced masonry models (Table 1); terms used in this table are defined in Appendix A. While load-displacement relationships, cracking patterns, and ultimate strength are often adopted as comparative parameters [as done by Lourenco et al.'s [13] for judging micro- versus macro-modeling strategies or by Chaimoon and Attard [14] for validating a simplified micro-modeling approach], this is not always the case.

TABLE 1-Comparative quantities in previous research.

Aspects	Nodal displacement	Nodal stress/strain	Load vs. displacement	Cracking pattern	Ultimate strength	Computational cost	Validation Type [(1)]
Lourenco et al. [13]			X	X	X		I
Chaimoon and Attard [14]			X	X	X		I
Truong-Hong & Laefer [15]	X					X	I
Roca et al. [16]			X		X		I
Zucchini & Lourenco [17]		X	X		X		I & II
Orduña & Lourenço [18]			X		X		II
Kappos et al. [19]	X					X	II
Sincraian & Azevedo [20]	X		X	X			II
Mohebkhah et al. [21]			X		X		II

The most common strategy has considered exclusively global response. For example, Truong-Hong and Laefer [15] assessed only nodal displacements at discrete measurable positions from a soil-structure interaction experiment, because of instrumentation accessibility issues, while Roca et al. [16] compared the general shear-lateral displacement relationship to determine global response and ultimate shear force when comparing an equivalent frame method to experimental results. In a not dissimilar approach, Orduña and Lourenço [18] validated a limit analysis on rigid blocks assemblages by considering the load-path response and the ultimate load factor (the ratio between the load causing collapse and the nominal value), while Mohebkhak et al. [21] adopted a more simplified strategy, looking at the collapse load and the deformation patterns to compare the efficiency of a discrete element method to experimental results. The focus on global response was also adopted by Kappos et al. [19] in their assessment of the relative accuracy of a simplified model for lateral analysis of UMB. In this case, the force-lateral displacement relationship was employed for optimizing analysis costs.

In contrast, Sincraian and Azevedo [20] looked at deformation patterns, crack openings, and sliding, as well as the relative displacement of the top of the model in benchmarking a discrete element method (DEM) versus a FEM one under seismic loading. This combined approach recognizes the influence of structural configuration, window position, and opening ratio (area of window/total possible wall area of solid wall) on a building's response [22,23]. Evaluation is made at individual points or more generally using graphical methods. In contrast, a more rigorous, statistics-based procedure such as relative or absolute error was proposed by Orduña and Lourenço [18].

When discussing the quality of auto- or semi-auto-generated FEM meshes derived from remote sensing data, there is an additional layer of complexity reflective of the fact that the remote sensing data capture approach harvests discrete points, as opposed to continuous information. This may result in small geometric inaccuracies, and additional ones may emerge when the data are transformed from individual points into a solid model. The resulting solid models may differ locally and/or globally from models derived from manual site survey. The quantification of such geometric discrepancies cannot be established without a measured survey and still fails to answer the more critical question, "To what extent do these discrepancies impact structural response". The following proposes a more inclusive benchmarking approach that addresses traditional concerns, as well as these emerging ones of assessing the influence of mildly discrepant geometries for historic building façades.

Proposed validation process

Previously, validation approaches were proposed to determine a level of reliability of approximate solutions in predicting realistic response of physical models, in which critical responses of structures were used (Table 1). Instead, in this work, an objective validation of solid models of masonry building facades that contain geometric discrepancies is proposed that encompasses not only the overall dimensions of a structure

[(1)] Type I: the proposed method vs. experiment; Type II: between two numerical methods

but also the dimensions and positions of various openings. Discrepancies in such areas impact a model's stiffness and may influence results. For example, Pickhaver [24] investigated how various opening positions and percentages changed building responses to tunneling-induced subsidence. Those results showed that while increasing the opening ratio had little effect on the global façade response, the resulting crack patterns and local damage concentrations differed. Therefore, in order to prove reliability of using solid modes reconstructed from TLS data in computational modeling, impacts of the geometric difference on the structural response must be investigated at both the local and global levels. For investigating those impacts, a new validation procedure is proposed (Fig. 1). The process compares the structural response of FEM models based on TLS post-processing to ones created from manual site surveys, in which the FEM models were subjected to self-weight and foundation movements due to construction of excavation. In fact, since the terrestrial units cannot capture roof data, the aerial units are of insufficient accuracy to adequately capture façade details for this type of processing (see [25] for a more extensive discussion of this). Also, none of auto or semi-auto approach has been developed to reconstruct interior objects of the building from such data. Currently, there is not a method for the automatic generation 3D building models reconstructed from such data. Furthermore, as the masonry buildings have weak, out-of-plane connection details and a high vulnerability to horizontal strain when oriented perpendicularly to a subsidence trough, to assess damage of building due to excavation/tunneling-induced settlement, analyzing two-dimensional (2D) wall has been considered as a reasonable compromise between accuracy and resource allocation compared to the high computational expense and complexity of three-dimensional (3D) models (e.g. [26-29]). Thus, the 2D building façade was interested in this validation. Comparative quantities involve the maximum structural response (called conventional validation) and usage of the FEM results in building damage assessment (called performance validation). In the conventional validation, comparative quantities involving the displacements, stress, and strain were selected, as they are primary parameters to assess structural responses. Local structural response is critical for accurate damage prediction, thus both global and local factors must be considered. Thus, the performance validation is proposed as the basis in which tilt, crack width, damage level, and a building damage ratio are considered for building models subjected to excavation-induced ground movements. Results of this validation show convergence of post-computational results. Consequently, details of comparative quantities in this proposed validation are discussed below.

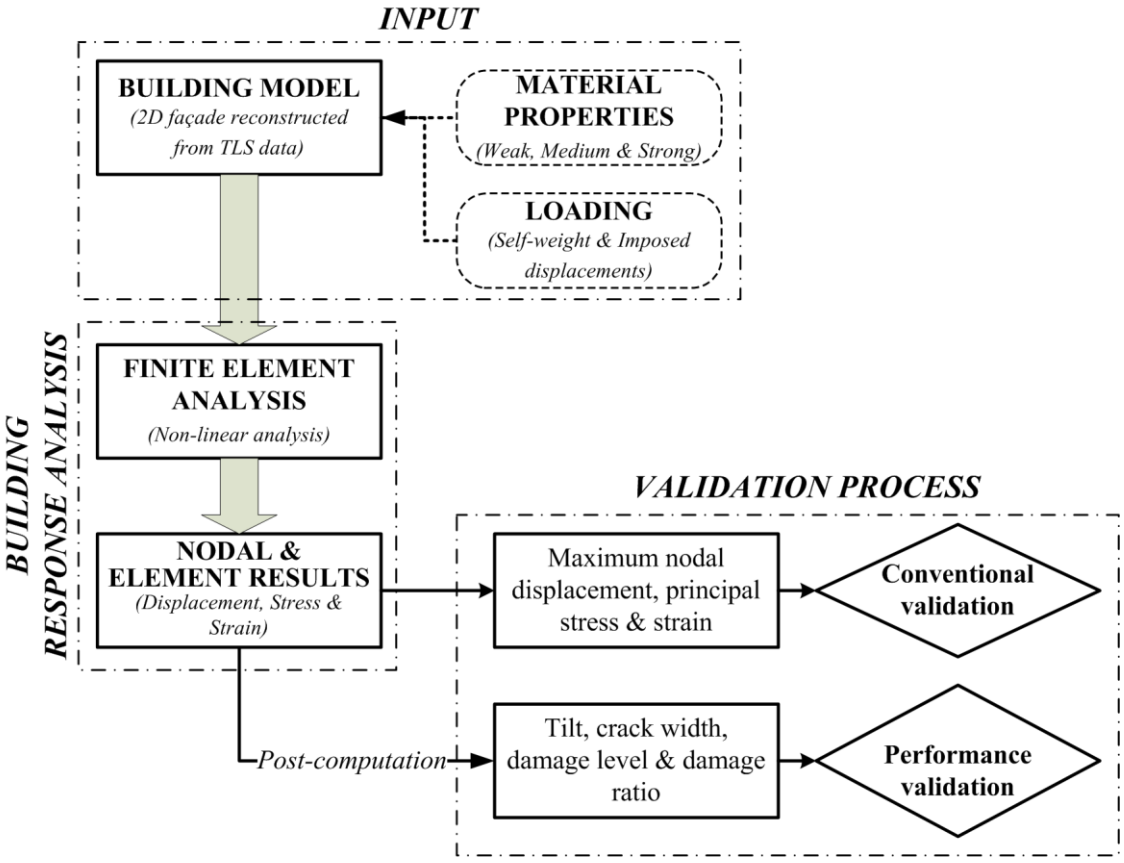

FIG. 1-Workflow of the proposed validation

Conventional validation

Similar to previous work, maximum nodal displacements, nodal stress, and strain obtained directly from FEM solutions are used to investigate the discrepancy of the overall response caused by differing geometries. To measure local behavior, the nodal displacements and the principal strain are selected at points of expected high stress-concentrations (e.g. corners of windows and openings), where damage is likely to commence.

UMB performance

For UMBs subjected to ground movement, their post-subsidence health is of concern. As such, the following categories of tilt, cracking width, damage level, and building damage ratio are proposed.

Maximum tilt

The relationship between load and displacement underlying a building's maximum tilt provides general behavioral information and is often used to predict damage in UMBs [30] (Eq. 1):

$$\omega = \frac{1}{n-1}\sum_{i=1}^{n}\frac{S_{h,i+1}-S_{h,i}}{L_{i,i+1}} \tag{1}$$

where $S_{h,i}$ and $S_{h,\,i+1}$ are the horizontal displacements of node i and i+1 respectively, $L_{i,i+1}$ is the distance between node i and i+1, and n is a number of nodes considered. For a building subjected to excavation- or tunneling-induced ground movements, the nodes along the building's edge perpendicular to the excavation face are selected.

Cracking patterns and widths

Cracking patterns and widths have long been used to characterize damage to buildings adjacent to construction activities [31]. Since smeared crack models are mesh-dependent, and because the FEM meshes differ due to small geometric discrepancies, a similar discretization mesh scheme is applied to both models. Subsequently, there are only minor differences of discretization errors between CAD-based models and remote sensing based ones, which do not affect the cracking characteristics. The cracking pattern can be obtained directly from the FEM results, but crack widths must be computed at the integration points of cracked elements from crack strain and characteristic length, as proposed by Bažant and Planas [32]:

$$w_{cr} = \varepsilon_{cr} h \tag{2}$$

where ε_{cr} and h are crack strain and characteristic length of elements, respectively.

The characteristic length should correspond to a representative dimension of the mesh size (e.g. [33-35]). The characteristic length generally depends on the element type, element size, element shape, integration scheme, and the specific problem. The characteristic length can be expressed as Eq. 3

$$h = \alpha\sqrt{\sum_{i=1}^{NINT}\gamma_i \det J_i} \tag{3}$$

where γ_i is the weighting factor of the integration rule, and $\det J_i$ is the Jacobian transformation between the local, iso-parametric coordinates and the global coordinate system for integration i, NINT is the number of integration points in each element, and α is a modification factor, which depends on the element type and integration scheme. Based on the studies by Oliver [35] and Scotta et al. [36], the herein adopted characteristic length was approximated according to Eq. 4.

$$h^{(e)} = \sqrt[m]{V^{(e)}} \tag{4}$$

where $V^{(e)}$ is the FE volume of the element; m is equal to 1, 2, 3 corresponding to one-, two- and three-dimensional analysis. However, in this work, as the cracking width was computed for each integration point of each cracked element, the volume of the integrated point was used in Eq. 4.

As the decomposed strain model is implemented to perform crack behavior and crack growth [37], the crack strain can be calculated based on an elastic-softening stress strain curve (Fig. 2) and the output stress

derived from the FEM results, as expressed by Eq.5.

$$\varepsilon_c = \varepsilon_t - \frac{\sigma}{E} \tag{5}$$

where e_{tol} and σ are, respectively, the total principal strain and principal stress at integration points of the cracked element, and E is Young's modulus.

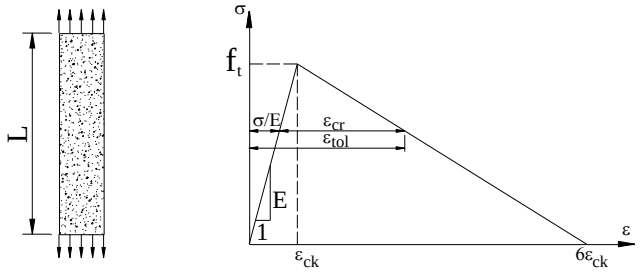

a) Homogenous bar b) Elastic-softening stress strain curve

FIG. 2-Response of homogeneous bar under uni-axial loading for computing the crack width based on a smeared crack model

Damage level and damage ratio

Various criteria, such as angular distortion [38], critical tensile strain [39,40] or cumulative crack width [41] are used to assess damage of buildings subjected to excavation/tunnel-induced ground movement. Herein, the degree of damage has been determined by comparing the maximum principal strain in the model to the critical tensile strain [42], while the building damage ratio is computed by the total volume of element damage over the building volume, where an element is considered as damaged, if the principal strain at its integration points exceeds the critical strain, $0.5x10^{-3}$ corresponding to a very slight damage level according to standard levels of severity within the tunneling community [42].

In summary, by using those comparative parameters (Table 2), the proposed validation process herein considers the impact of discrepant geometries on the overall response and local behaviors. For measuring the impact of the overall building response, absolute and relative differences are recommended (Eq.s 6 and 7, respectively):

$$\text{Absolute error} = x^{CAD} - x^{RS} \tag{6}$$

$$\text{Relative error} = \frac{x^{CAD} - x^{RS}}{x^{CAD}} x100 \tag{7}$$

where x^{CAD} and x^{RS} are the parameters derived from FEM models from a CAD drawing and Remote Sensing (RS) data, respectively, which involve the maximum displacements, stress, strain, tilt, crack width, and building damage ratio.

TABLE 2-Proposed comparative quantities for validating geometric solid models.

	Conventional validation		Validation performance			
Aspects	Nodal displacements [(1)]	Nodal stress/strain [(1)]	Load vs. displacement (tilt)	Cracking width	Damage level	Ratio of building damage
Overall response	X	X	X	X	X	X
Local response	X	X				

However, for comparing parameters (nodal displacements and nodal principal strain) representing local behavior, the validation metric is used to describe difference between FEM models [11,43]. For that, FEM results are assumed as random samples in the form of a normal distribution, where CAD-based and RS-based models are respectively (x_1^{CAD}, x_2^{CAD}, . . ., x_n^{CAD}) and (x_1^{RS}, x_2^{RS}, . . ., x_3^{RS}). The sample mean and standard deviation of individual differences of numerical results between the FEM models are given in Eq.s 8 and 9 [44].

[(1)] for validating overall response, the maximum nodal values are used

$$\bar{x} = \frac{1}{n}\sum_{i=1}^{n}\left(x_i^{CAD} - x_i^{RS}\right) \quad (8)$$

$$s = \sqrt{\frac{\sum_{i=1}^{n}\left[\left(x_i^{CAD} - x_i^{RS}\right)^2 - \bar{x}\right]^2}{n-1}} \quad (9)$$

where n is a number of random samples in the population.

Based on this statistical procedure, with a predefined the level of confidence, the limit of agreement between the individual differences can be expressed as Eq. 10.

$$\mu \approx (\bar{x} - t_{\alpha/2}\frac{s}{\sqrt{n}}, \bar{x} + t_{\alpha/2}\frac{s}{\sqrt{n}}) \quad (10)$$

where $t_{\alpha/2}$ is 1-α/2 quartile of the t-distribution for v=n-1 degree of freedom and 100(1-α)% is the level of confidence. In this work, the t-distribution is selected to estimate error bounds, as this distribution is suitable with a small number of sample observation, and the cumulative t-distribution differs from the cumulative standard distribution by less than 0.01 for all quantities when n is greater than 16.

Geometric building model generation

TLS data acquisition and building model creation

The selected validation case is an in-plane analysis of UMB facades subjected to an adjacent excavation, with consideration for three classes of material strength (i.e. weak, medium, and strong). To test the proposed approach, three relatively flat, masonry façades of simple morphology were chosen in Dublin, Ireland to demonstrate the validation process. Buildings 1 and 2 were four-storey and relatively narrow, while Building 3 was six-storey and significantly larger (Fig.s 3a, 4a and 5a). Since scanning density impacts both the time for data collection and post-processing, as well as storage requirements, there is often a trade off between scan density and fiscal limitations. In this study, Buildings 1 and 2 were scanned at a 10 mm resolution with a Trimble GS200 scanner [45], in which the standard deviation for the scanner was ~2.5 mm at a scanned range of 100 m. The scanning time was around 35 minutes for each. To obtain the same resolution for Building 3, the projected time for data collection would have been closer to two and a half hours. Due to access issues, traffic, and related interferences, this was not considered viable. Therefore, the resolution of 20mm was selected to reduce the data collection time and so that the scans could be done without interference. The final scanning time for this building was 1 hour and 20 minutes. . Subsequently, the original scanned data, which contained terrain features and internal objects/walls, in addition to each building's facade, were registered and manually cleaned of irrelevant points within the Trimble GS200's software, RealWorks Survey Advanced (RWS) V6.3 [46]. See Truong-Hong et al. [47] for detailed processing information. The remaining points were projected onto a fitting plane before applying the FacadeDelaunay (FD) algorithm [47]. Therefore, noise in the point clouds was not found to be a major problem in the subsequent building reconstruction.

To determine minimum data collection requirements for building reconstruction, various derived data densities were used as input sets for the FD algorithm. While those data sets could have been achieved by rescanning the building at the same position three other times, due to the potential interference of traffic and other visual obstacles, the re-sampling process was selected instead of rescanning at a lower resolution. Thus, each façade was randomly re-sampled from the original scanned data set to 175 pts/m^2 (expected distance between sampling points is 75 mm) (Fig.s 3b, 4b and 5b). In this process, the initial reference point was randomly picked by the RWS V6.3 program, and then all points within the threshold distance to the reference point were removed from the data set.

These various data sets were used as input for the FD algorithm developed by the authors [47]. That algorithm automatically extracts boundary points of building features (Fig.s 3b, 4b and 5b) and then generates solid models of the building façades (Fig.s 3c, 4c and 5c). As geo-referencing was not assigned during data collection, the RS-based model and CAD-based ones were not co-registered prior to determining geometric discrepancies. The drawbacks of such a comparison were addressed in detail elsewhere [48]. In this valida-

tion, the local coordinate system of each model was roughly assumed as the lower left corner of the model. The statistical procedure has been conducted to measure dislocation of parts of the building model-based TLS data against ones-based CAD drawings. Differences of coordinates of two opposite corners (a lower left and upper right corners) of openings were examined, in which x- and y-axes were respectively assigned to the horizontal and vertical directions. A summary of absolute errors of the coordinates is presented in Table 3. For more details see Truong-Hong et al. [47]. The minimum dislocation of openings found in Building 1 was -39.8 mm [Standard deviation (SD)=67.9 mm] while the maximum ones in Building 3 was 103.4 mm (SD=57.6 mm).

TABLE 3- Coordinate differences between CAD drawings against the FD -based solid models

Aspect	Building 1	Building 2	Building 3
Average (mm)	-39.8	58.7	103.4
Minimum error (mm)	-171.4	-130.0	0.0
Maximum error (mm)	55.8	185.8	194.1
Standard deviation (mm)	67.9	81.6	57.6

Furthermore, compared to CAD-based solid models, the RS-based ones slightly underestimated the overall dimensions (height and length): the maximum relative error was 1.1% for Buildings 1 and 2 and 0.6% for Building 3 (Table 4). Opening areas in the RS-based solid models differed by no more 4% (<1.38 m^2 in Building 2) (Table 4).

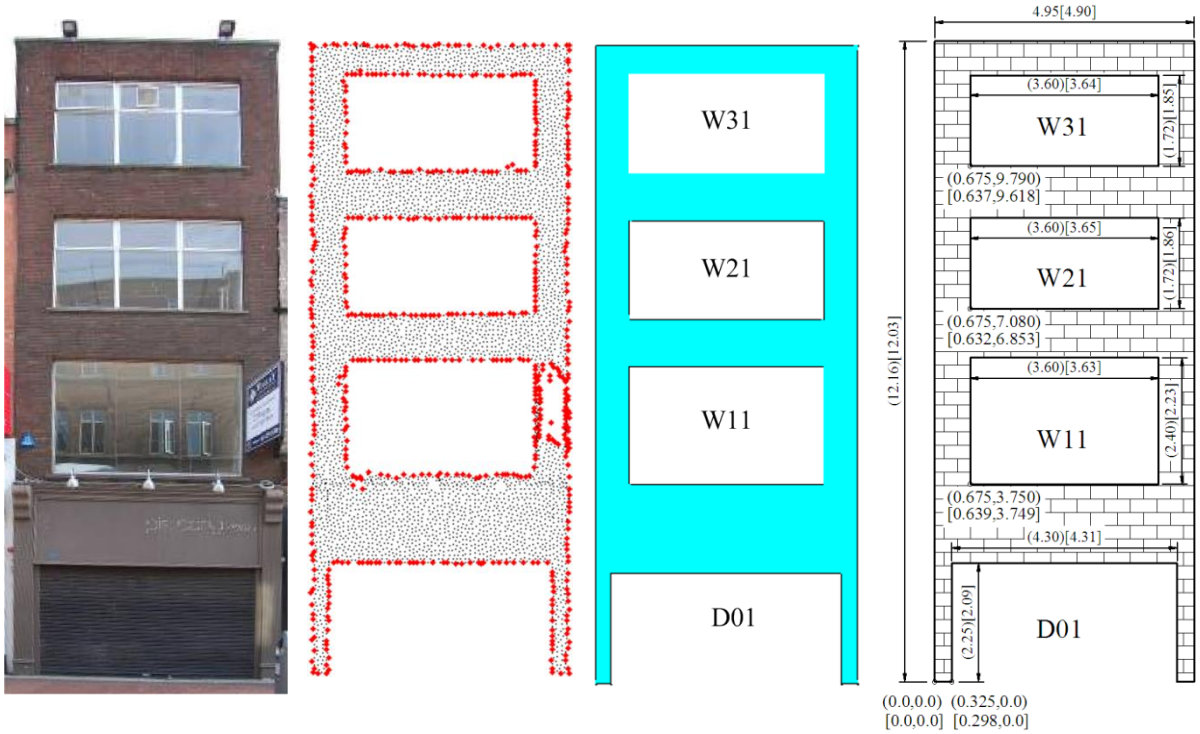

a) Photograph b) Sampling data set and boundary point detection c) Solid model in ANSYS d) CAD drawing

FIG. 3-Post-processing TLS data for Building 1: 2 Anne St. South (26 4931 points in original set, and 4,643 points in re-sampled dataset)[(1)]

[(1)] values in [] are of building models derived from the FD algorithm, while values in ( ) are the measured values

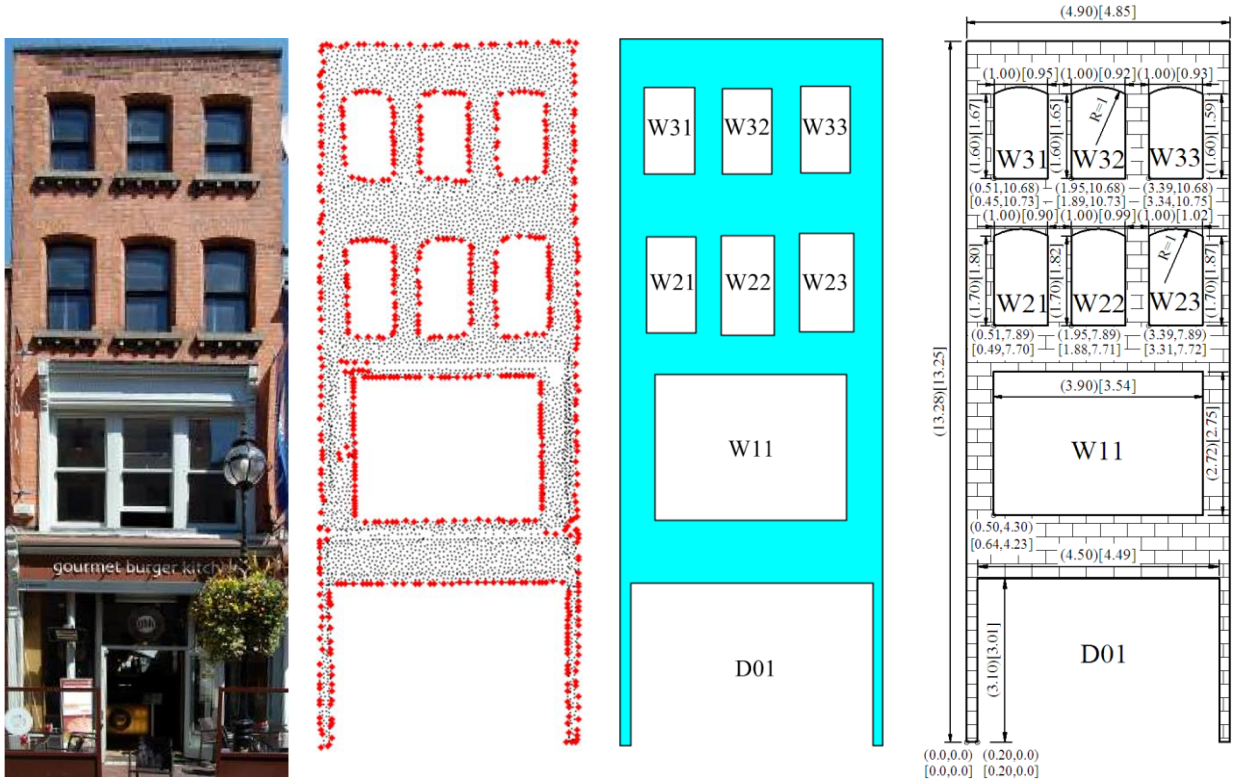

a) Photograph b) Sampling data set and boundary point detection c) Solid model in ANSYS d) CAD drawing

FIG. 4-Post-processing TLS data for Building 2: 5 Anne St. South (190,865 points in original set and 5,366 points in re-sampled dataset)[(1)]

TABLE 4-Derived overall dimensions of the building models

Building	Sources	Façade information		
		Width, m	Height, m	Opening area, m^2
Building 1 (B1): 2 Anne St. South	CAD	4.95	12.16	30.7
	RS FD algorithm	4.90	12.03	30.6
Building 2 (B2): 5 Anne St. South	CAD	4.90	13.28	34.5
	RS FD algorithm	4.85	13.25	33.2
Building 3 (B3): 2 Westmoreland St.	CAD	19.36	17.00	96.2
	RS FD algorithm	19.27	16.90	97.6

Using the lower-left corner of the façade and its openings as local origins, the average absolute errors of opening dimensions were calculated as less than 11.0 mm [Standard deviation (SD)=121.9 mm] (B2FD) for the small buildings and greater than 14.5 mm (SD=50.1 mm) for the large building (Table 5). However, the smallest absolute difference was 39 mm (B3FD), and the largest was 360 mm (B2FD). In terms of opening position, average errors were respectively 68.0 mm (SD=83.9 mm), 58.7 mm (SD=84.5 mm), and 99.8 mm (SD=57.6 mm) for Buildings 1, 2, and 3 (Table 5). These errors were data driven and caused by sample points on a canopy atop a door, articulated window ledges, and wide window frames.

TABLE 5-Geometric differences between CAD drawings against FD-based solid models

Aspects	Opening size, mm			Opening position, mm		
	Building 1	Building 2	Building 3	Building 1	Building 2	Building 3
Average	-6.4	11.0	-14.5	68.0	58.7	99.8
Minimum error	-208.0	-360.0	-39.0	-226.7	-185.8	-194.1
Maximum error	98.0	168.0	162.0	0.0	130.0	0.0
Standard deviation	118.1	121.9	50.1	83.9	84.5	57.6

[(1)] values in [] are of building models derived from the FD algorithm, while values in ( ) are the measured values

a) Photograph

b) Sampling data set and boundary point detection

c) Solid model in ANSYS

d) CAD drawing

FIG. 5-Post-processing TLS data for Building 3: 2 Westmoreland St. (650,356 points in original set and 35,468 points in re-sampled dataset)[(1)]

Building response analysis

To establish the relative influences of mildly discrepant geometries, sample solid models were tested with a range of material properties, as described below.

Software, modelling strategy, element type, and material constitute law and properties

A non-linear analysis was employed to determine responses of the models by mean of the advanced finite element analysis package, ANSYS [37]. A macro-modeling strategy was adopted as detailed elsewhere [15,49], in which a 3D SOLID65 element with eight nodes associated with three degrees of freedom at each node, isotropic behavior, and 2x2x2 integration points was used to model entire building models [37]. Non-linear analysis was conducted with a William-Warnke failure criterion [50] and a Drucker-Prager yield criterion [51] for tensile and compressive behavior, respectively.

Since mechanical properties cannot be detected from LiDAR data, they selected from the peer-reviewed literature and experimental results were adopted in a validation process; see Truong-Hong [48] for details. Three sets of materials were used (Table 6). Additionally, the internal friction angle and the dilatancy angle for performing Drucker-Prager yield criterion were assumed to be 35^o and 10^o, respectively [52,53], while the internal cohesion was calculated from experimental tests on the compressive strength and the internal friction angle [15].

[(1)] values in [] are of building models derived from the FD algorithm, while values in ( ) are the measured values

TABLE 6-Composite material properties from published literature

Aspect	Young's modulus (E), MPa	Poisson's ratio, ν	Compressive strength (f_c), MPa	Tensile strength (f_t), MPa	Internal cohesion (c), MPa
Average value	3,465	0.17	20.55	0.74	-
Minimum value	1,260	0.07	4.10	0.05	-
Maximum value	5,700	0.26	48.20	2.24	-
Standard deviation	1,531	0.05	12.60	0.54	-
Number of samples	16	11	50	20	-
Weak material (M1)	1,260	0.07	4.10	0.05	1.07
Medium material (M2)	3,480	0.16	26.15	1.27	6.81
Strong material (M3)	5,700	0.26	48.20	2.24	12.55

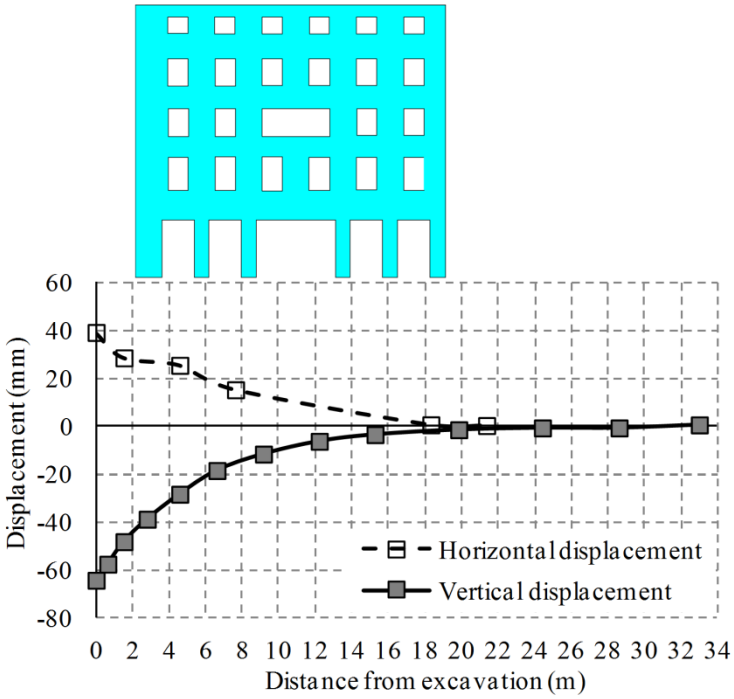

FIG. 6-Free field scaled trough settlement profile adopted as input for validation

Generating FEM mesh, loading and numerical control

Unstructured hexahedral meshes were adopted with an element size equal to 0.15m for Buildings 1 and 2 and 0.25m for Building 3 (Table 7). In FEM, accuracy of nodal results (stress, strain, and displacement) depends in part on sufficient mesh density, but this is a well-known topic outside the scope of this work. Herein, each building was subjected to experimentally induced foundation settlements as described elsewhere [54] converted to the prototype scale (Fig. 6). These values were imposed on the bottom of the building façade as constrained displacements applied in multiple, sub-load steps. The building was assumed to be 2 m behind the excavation face. Self-weight was based on mass density, gravity acceleration, and model volume.

TABLE 7-Statistics of the FEM meshes[(1)]

Building	CAD-based		RS FD-based	
	Nodes	Elements	Nodes	Elements
Building model 1 (B1)	4,791	2,712	4,575	2,566
Building model 2 (B2)	5,193	2,874	5,178	2,862
Building model 3 (B3)	12,969	7,690	13,548	8,022

Validation of numerical results

[(1)] FEM meshes from the FD algorithm and the CAD model differed slightly because of discrepancies in their underlying geometries.

Maximum displacement, stress, and strain

When comparing the maximum FEM displacements of the CAD-based and FD-based meshes, relative errors were mostly less than 3.7% (Table 8), except for 9.6% for the maximum horizontal displacement (B3CADM1 vs. B3FDM1). However, the absolute difference was no more 4.1 mm (B3CADM1 vs. B3FDM1). The maximum horizontal displacement error was generally greater than the vertical. For example, Building 2 with weak material had a -1.3% error in horizontal displacement but only -0.5% in the vertical. Overall, the relative errors with the weak material were larger than with stronger materials.

TABLE 8-Maximum displacement, principal stress, and strain 1 in the building models

Model	Displacements		Maximum principal stress 1 [(1)], MPa	Principal strain 1 (x1e-3)	Maximum crack width, mm	Tilt (x1e-3)	Damage category [(2)]
	UX, mm	UY, mm					
B1CADM1	90.655	47.485	1.494	13.251	1.178	5.580	4 & 5
B1FDM1	90.448	47.480	1.487	15.440	1.317	5.608	4 & 5
B1CADM2	88.696	45.265	9.471	5.059	0.363	5.408	4 & 5
B1FDM2	88.346	45.267	9.458	4.474	0.353	5.438	4 & 5
B1CADM3	88.033	44.603	17.522	5.560	0.399	5.352	4 & 5
B1FDM3	87.729	44.688	17.497	5.209	0.403	5.383	4 & 5
B2CADM1	95.121	50.424	1.423	10.961	0.950	5.474	4 & 5
B2FDM1	96.366	50.688	1.398	13.896	1.160	5.652	4 & 5
B2CADM2	95.985	46.444	9.351	3.249	0.230	5.496	4 & 5
B2FDM2	96.463	46.552	9.351	3.286	0.217	5.563	4 & 5
B2CADM3	96.059	45.616	17.319	3.419	0.233	5.500	4 & 5
B2FDM3	96.477	45.691	17.345	3.413	0.217	5.553	4 & 5
B3CADM1	42.552	35.763	1.542	38.423	4.692	1.583	4 & 5
B3FDM1	46.653	36.995	1.536	51.922	5.810	1.737	4 & 5
B3CADM2	36.614	26.996	9.865	46.271	5.488	1.308	4 & 5
B3FDM2	37.570	27.993	9.960	43.465	5.059	1.356	4 & 5
B3CADM3	37.357	26.299	18.209	47.032	5.547	1.347	4 & 5
B3FDM3	37.359	26.525	18.161	46.091	5.367	1.352	4 & 5

When a smeared crack model is employed, the principal stress 1 always decreases along a softening branch, after exceeding the tensile strength (Fig. 2b). Thus, a comparison makes sense, only if the smeared crack model is deactivated for this aspect. In this, the relative errors were no more than 1.8% (B2CADM1 vs. B2FDM1). Additionally, the maximum absolute errors were less than 0.192 MPa. Graphically, a distribution of the principal stress 1 in FEM models of the same building façade was similar in pattern, although their values differed slightly (Fig. 7).

In validating maximum strain, the principal strain 1 was derived from non-linear analysis. For this a smeared crack model was used. Relative errors were significantly higher for the FD-model when a weak material was used: -16.5% for Building 1, -26.8% for Building 2 and -35.1% for Building 3. With a medium or strong material, the relative errors were generally no more 6.3% (B1CADM3-strong vs. B1FDM3-strong) except for 11.6% (B1CADM2-medium vs. B1FDM2-medium).

Maximum tilt

A maximum tilt due to excavation-induced foundation movements and self-weight for each FEM model is shown in Table 8, in which relative errors were mostly less than 4.38%, except for 9.76% for Building 3. Generally, the differences between FD models with a weak material were larger than with other materials. For example, the relative errors of Building 2 were -3.07%, -1.21% and -0.95% when weak, medium, and strong materials were used, respectively. In conclusion, the maximum absolute difference of 0.177×10^{-3} [B2CADM1 vs. B2FDM1] corresponding to 1/5650 did not affect building assessment as compared to the maximum design limit value of the tilt for low-rise buildings of 1/400 [30].

[(1)] Principal stress 1 was used to assess safety, because of the low tensile strength of UMBs.

[(2)] 4 = Severe damage; 5 = Very severe damage

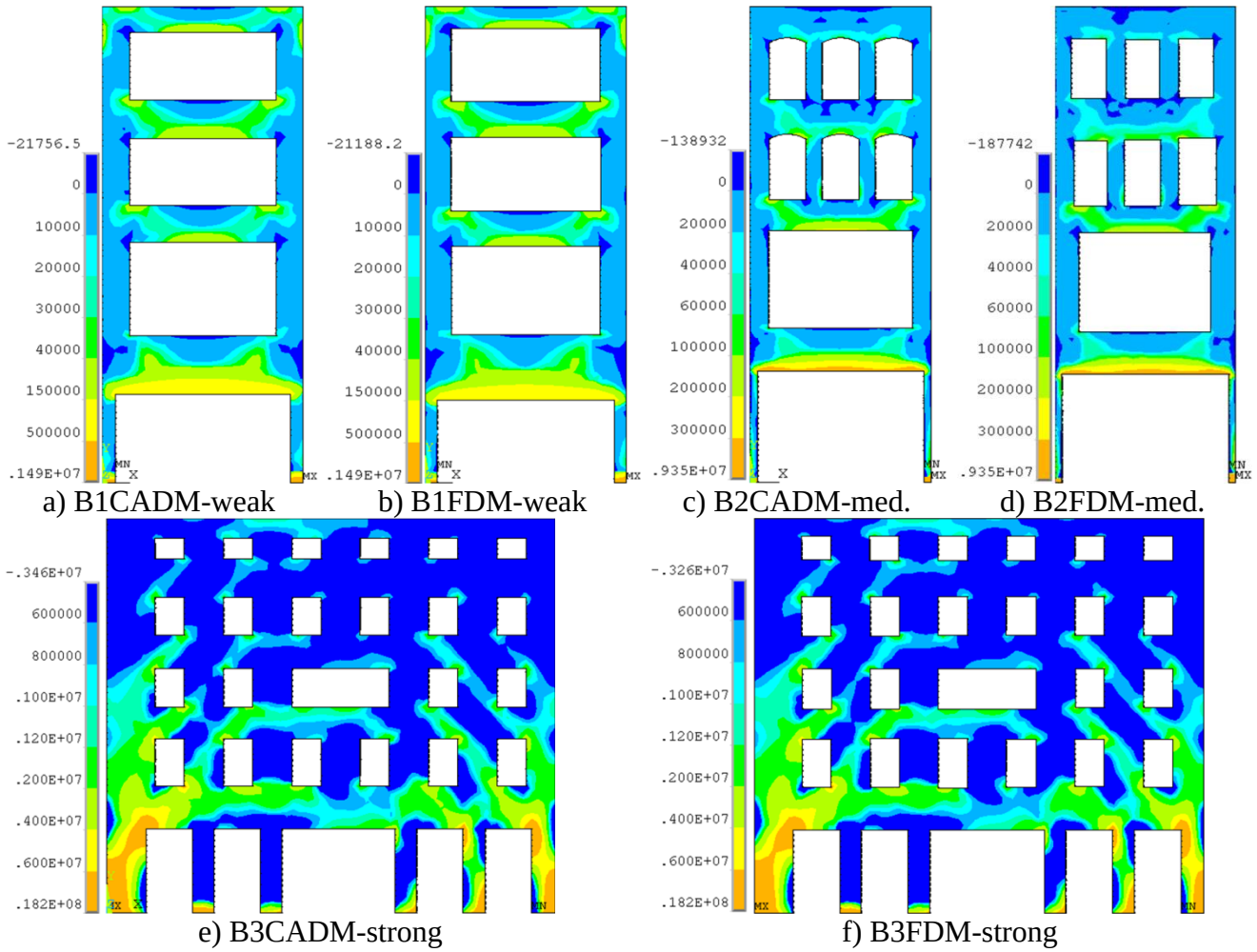

a) B1CADM-weak b) B1FDM-weak c) B2CADM-med. d) B2FDM-med.

e) B3CADM-strong f) B3FDM-strong

FIG. 7-Examples of distribution of principal stress 1 under self-weight and imposed displacements

Cracking patterns and width

Generally, cracking pattern distributions were in good agreement (Fig. 8) with cracking patterns in the FD-based models generally slightly wider than the CAD-based ones. Comparing the crack width against load increment, showed good agreement (Figure 9). The relative errors of the crack width were up to 23.5% for FEM model with a weak material but no more 7.82% for FEM models with other materials. However, the maximum absolute differences were 1.12 mm (B3CADM1 vs. B3FDM1) for the weak material, while they were 0.43 mm (B3CADM2 vs. B3FDM2) for the other materials (Table 8).

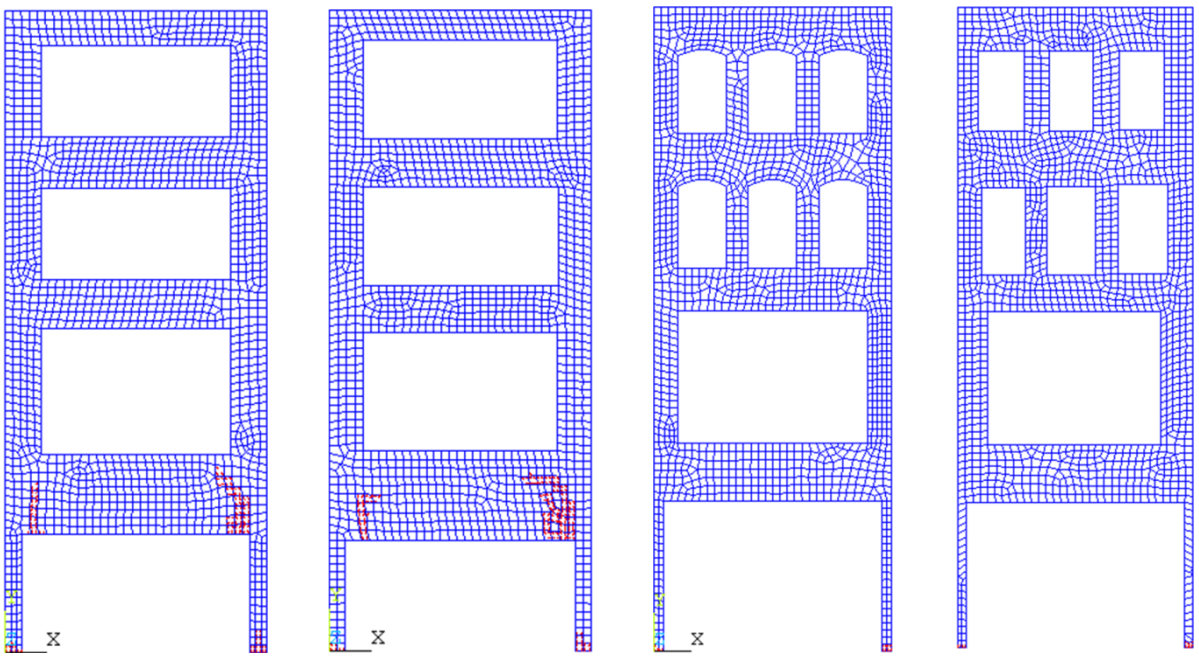

a) B1CADM-weak b) B1FDM-weak c) B2CADM-medium d) B2FDM-medium

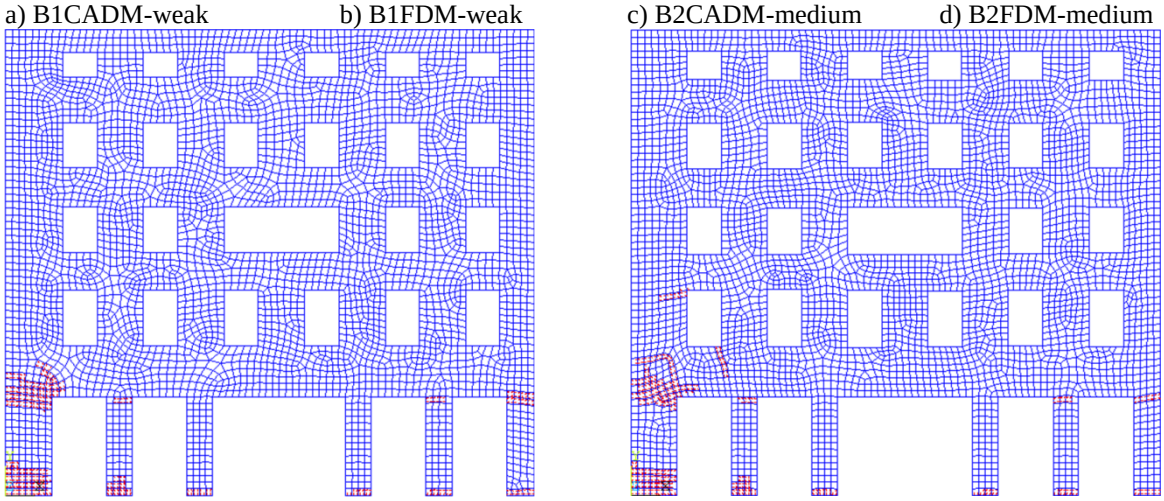

e) B3CADM-strong f) B3FDM-strong

FIG. 8-Cracking patterns in FE models due to self-weight and imposed displacements

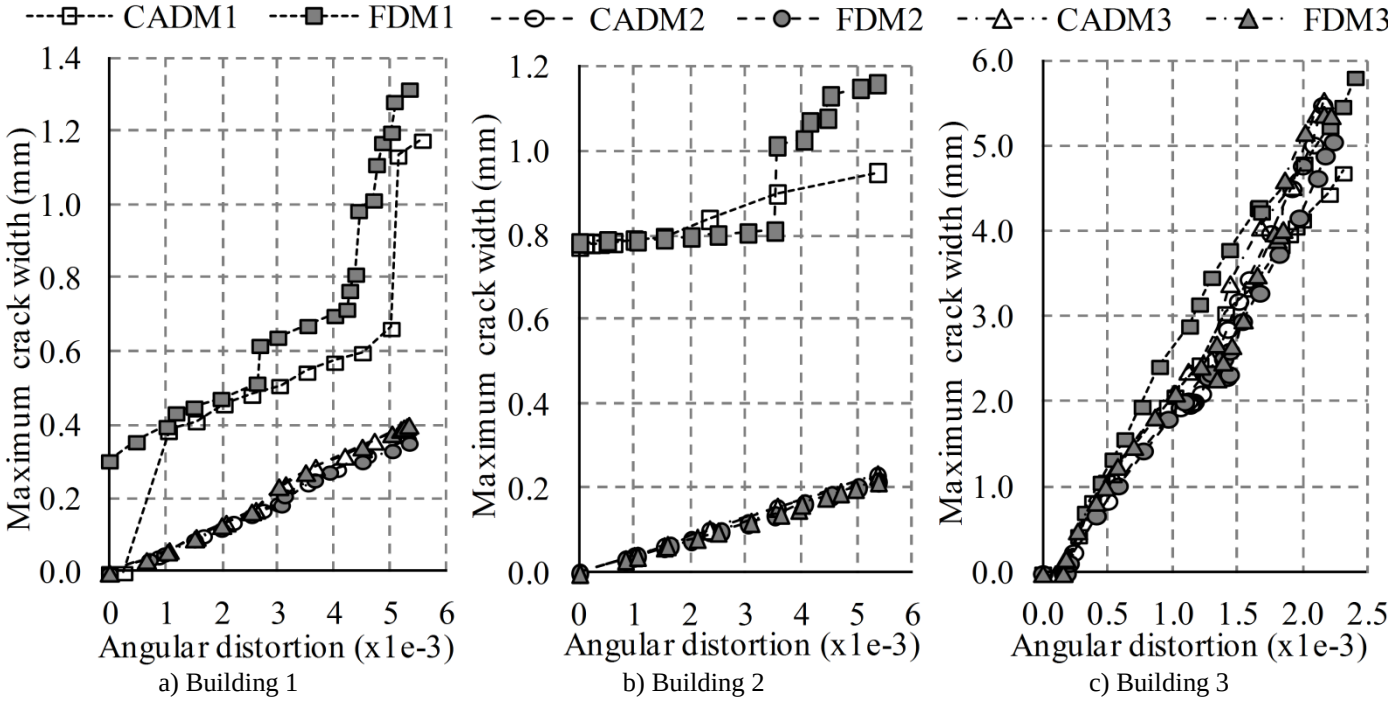

a) Building 1 b) Building 2 c) Building 3

FIG. 9-Increasing crack widths

Damage level and damage ratio

Employing the state of strain theory [42], principal strain 1 was compared to the limiting tensile strain. All models garnered damage levels of 4 & 5 (severe and very severe) according to Burland [31] (Table 8). For computing a building damage ratio, the volume of integration point was considered damaged, if the maximum principal strain 1 at the integration point exceeded the critical tensile strain of damage category 1 [42]. The maximum difference was no more 1.0% (B2CADM1 vs. B2FDM1), and the minimum was 0.03% (B2CADM2 vs. B2FDM2) [Fig. 10]. For the non-weak material, the maximum difference was only 0.3% (B3CADM2 vs. B2FDM2).

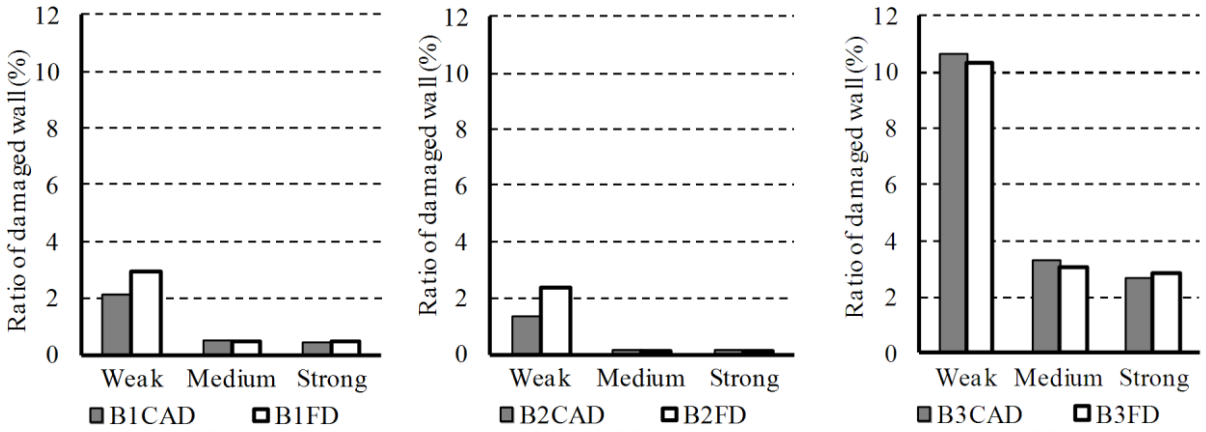

a) Building 1 b) Building 2 c) Building 3

FIG. 10-Ratio of damaged vs. undamaged wall areas

Local behaviour via nodal displacements and strains

Correlations of local behavior (nodal displacement and principal strain) between FEM models with identical materials are shown in Table 9, based on a 90% confidence level. Generally, the "limit of agreement" (Eq. 10) of the horizontal displacement had a substantially wider response range than the vertical ones. The largest range of horizontal displacements was 1.634±0.346 mm (SD=1.576 mm) [Building 3-weak], while it was only 0.615±0.155 mm (SD=0.378 mm) [Building 2-weak] for the vertical. The maximum absolute difference between the horizontal and vertical displacements was 5.732 mm (Building 3-weak) and 3.644 mm (Building 3-strong), respectively. The FEM models with the weak material gave a wider limit range than those with other materials. For example Building 2, the agreement limit of the horizontal displacements 0.449±0.152 mm (SD=0.370 mm) and for the weak 0.940±0.175 mm (SD=0.427 mm) for the strong materials, while ones of the vertical displacement were 1.352±0.282 mm (SD=0.688 mm) and 0.469±0.170 mm (SD=0.414 mm), respectively.

Discussion

Non-structural members (e.g. canopies, window ledges) or terrain in front of a building may interfere with data collection; for more details on the influence of these elements on the accurate reconstruction of building models from point clouds [47]. In the test cases herein, the geometric discrepancies had both direct and indirect impacts on the loading. A direct impact related to self-weight as function of volume of the building model. For instance, the 4% decrease in the surface area of Building 1 and 1.1% decrease for Building 2 lead to a proportional lessening of weight in that proportion as compared to the CAD-based models. An indirect impact related to imposed displacements is based on the building's relative position within the settlement trough. For Building 1, the 1.1% decrease in façade width caused only a 0.6% increase in angular distortion over the CAD-based model (5.16×10^{-3} vs. 5.13×10^{-3}), but with Building 3, the relatively smaller 0.5% difference in façade width caused a 3.8% increase in angular distortion of imposed displacements over the CAD-based model (2.85×10^{-3} vs. 2.75×10^{-3}) because Building 3 spans over both the hogging and sagging regions of the settlement trough. Despite increasing angular distortion, the maximum displacements and maximum principal stress 1 in FD-based models are mostly smaller than those in CAD-based models because of the FD-based models occupy less of the settlement trough than CAD-based models. Furthermore, as the building height in the FD-based models are shorter than ones in CAD-based model, the tilts in FD-based models are greater than those in CAD-based models. Since geometric discrepancies occur in lengths,

heights, and opening areas, prejudging which factor may dominate discrepant building response is nearly impossible. This is especially true as there are both direct and indirect impacts on the loading and overall stiffness. The concept of equivalent stiffness was proposed by Pickhaver [24] to investigate the influence of different geometries on the structural response of the buildings. Using this approach, relative errors of building stiffness were found to be -1.6%, -0.5, and +3.9%, respectively for Buildings 3, 1, and 2. The maximum and average displacements and principal strain 1 (shown in Table 8 and 9) are shown in Fig. 11. In general, average absolute errors of nodes of interest are smaller than absolute errors of nodes causing maximum responses, except for vertical displacements of Building 1 and 2 with the medium and strong materials (Fig. 11).

TABLE 9-Statistics of different nodal results between pairs of FEM models for each Building

	Weak Material			Medium Material			Strong Material		
Aspects	UX, mm	UY, mm	Strain 1 (x-1e-3)	UX, mm	UY, mm	Strain 1 (x-1e-3)	UX, mm	UY, mm	Strain 1 (x-1e-3)
				Building 1					
Average error	0.113	0.000	-0.055	0.177	-0.002	-0.004	0.159	-0.064	-0.044
Minimum error	-1.368	-0.234	-0.579	-1.283	-0.234	-0.034	-1.309	-0.566	-0.434
Maximum error	0.897	0.633	0.015	0.744	0.637	0.006	0.808	0.652	0.004
Standard deviation	0.631	0.247	0.184	0.617	0.253	0.012	0.630	0.326	0.137
$t_{5\%}\frac{s}{\sqrt{n}}$	0.366	0.143	0.107	0.358	0.147	0.007	0.365	0.189	0.080
				Building 2					
Average error	-1.448	-0.899	-0.034	-0.528	-0.521	-0.002	-0.449	-0.469	-0.004
Minimum error	-1.876	-1.991	-1.386	-1.031	-1.380	-0.035	-0.968	-1.309	-0.047
Maximum error	0.560	0.414	0.726	-0.031	0.611	0.013	0.069	0.650	0.008
Standard deviation	0.560	0.515	0.378	0.357	0.417	0.011	0.370	0.414	0.014
$t_{5\%}\frac{s}{\sqrt{n}}$	0.230	0.211	0.155	0.146	0.171	0.005	0.152	0.170	0.006
				Building 3					
Average error	-1.663	-0.250	0.016	-0.567	-0.394	0.055	-0.025	-0.300	-0.025
Minimum error	-5.732	-1.905	-5.113	-1.478	-1.694	-0.808	-2.331	-3.644	-1.182
Maximum error	0.116	1.676	11.741	1.930	0.003	2.895	0.184	-0.059	0.696
Standard deviation	1.554	0.701	1.949	0.411	0.302	0.417	0.313	0.453	0.208
$t_{5\%}\frac{s}{\sqrt{n}}$	0.346	0.177	0.428	0.090	0.066	0.091	0.069	0.099	0.046

As expected, buildings with the weak material are more impacted by small changes in relative stiffness, especially in the horizontal displacement (Fig.11a) and in the principal strain 1 (Fig.11c). As such, for Building 3, the absolute difference of the maximum horizontal and vertical displacements to the maximum imposed ones are, respectively, around 4% (1.23 mm vs. 28.26 mm) and 9% (4.01 mm vs. 44.49 mm), while the absolute difference of the principal strain 1 is 13.499x1e-3.

For Buildings 1 and 2 with medium and strong materials, the absolute error of the maximum displacements were mostly less than 1 mm, with the maximum horizontal displacements around 3% (0.956 mm vs. 28.26 mm) of the maximum imposed horizontal displacement. Similarly, for these same cases, errors of principal strain 1 were less than 1.6 times ($0.585x10^{-3}$ vs. $0.365x10^{-3}$) of the crack strain of the medium material. Those displacement errors were with the allowable discretization error (often 5-15%) during FEM mesh generation [55]. The second point of interest was that the 3.9% increased stiffness of Building 2 had a much smaller impact on relative errors than the 1.6% decreased stiffness of Building 3. By checking these trends against opening ratios and building widths, it became clear that the relative trough position was in this case the controlling factor, more than any direct geometric discrepancy.

In terms of the nodal principal strain, the agreement limit varied from $-0.016x10^{-3}\pm0.428x10^{-3}$ ($SD=1.949x10^{-3}$) [Building 3-weak material] to $0.044x10^{-3}\pm0.080x10^{-3}$ ($SD=0.137x10^{-3}$) [Building 1-strong material]. The largest difference in nodal principal strain was approximately 1.2 times the crack strain of the

medium material, $0.365x10^{-3}$ (f_t=1.27 MPa; E=3 480 MPa).

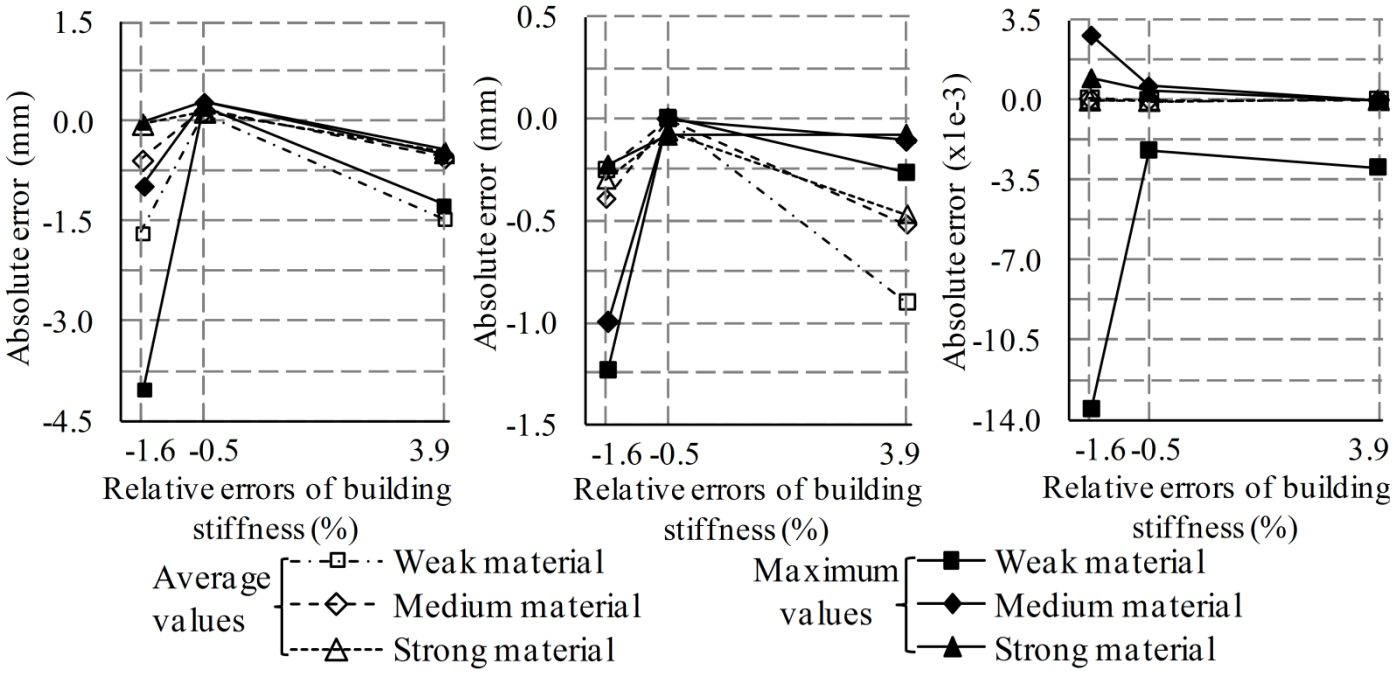

a) For horizontal displacements b) For vertical displacements c) For principal strain 1

FIG. 11-Comparing the absolute errors of the maximum and average displacement and principal strain 1 in FEM against relative errors of building stiffness due to geometric discrepancies

Similarly, Building 3's maximum principal stress 1 and tilt were more impacted than those of Buildings 1 and 2, particularly when the weak material was used (Fig. 12). As expected, when medium and strong materials were used, the relative errors of the principal stress 1 and the tilts were respectively no more 0.15% and 1.22% for the building models' overestimated stiffness. Consequently, with properties of common material, there are only small differences of FEM results from CAD-based models and FD-ones due to geometric discrepancies and those errors are within allowable standard errors.

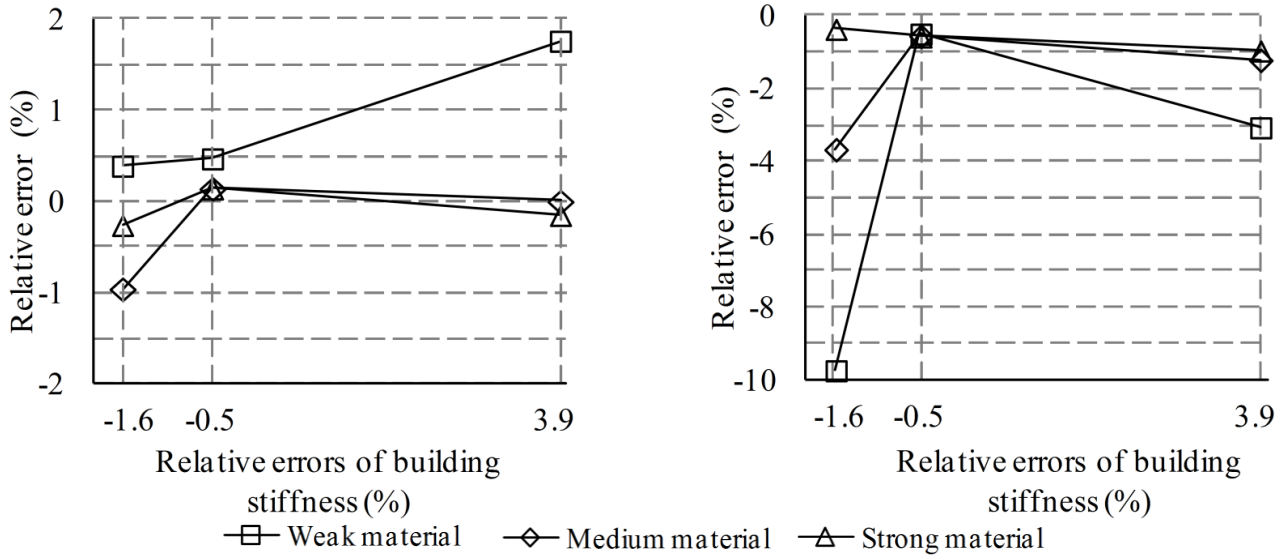

a) For principal stress 1 b) For maximum tilt

FIG. 12- Comparing the relative errors of the maximum principal stress 1 and tilts in FEM against relative errors of building stiffness due to geometric discrepancies

Since, the facade models derived from remote sensing data differed from on-site surveys in terms of the relative errors of length, height and opening area, and the maximum relative error of overall dimensions (height and length), predicting the relative impact of each divergence is nearly impossible, because these parameters affect not only stiffness of the model but also both direct and indirect impacts on the loading. As such, the TLS data based models must be investigated in terms of global and local responses to prove the us-

ability of these models. Interestingly, the proposed validation process explicitly showed that while the geometric discrepancies generated during data acquisition and processing did not affect the global responses (e.g. maximum displacements), they did impact local responses (e.g. crack distribution, vertical displacements atop windows).. Furthermore, in some cases, absolute errors of quantities representing local behavior were higher than global ones implying that restricting validation to global parameters fails to express fully the impact of mildly inaccurate geometries in building responses. Additionally, addressing divergence of local responses can reduce misleading local damage prediction. For example, in Building 2, if the local damage was predicted based on the global responses, the prediction may have been unconservative, because errors in the local responses were larger than the global ones (Fig. 11b). Therefore, this study provided detailed differences of building responses due to geometric inaccuracies, which can help structural engineers to decide on the appropriateness (or lack thereof) of the use of TLS data as the basis for their computational models.

Conclusions

A new validation process is proposed to establish differences in FEM results due to small geometric discrepancies of the solid models derived from remote sensing data from terrestrial laser scanning. The validation is conducted by comparing building responses based on building geometries obtained from independent manual surveys and from author collected TLS data. The subsequent buildings were ascribed the same material properties, loadings, and mesh discretization scheme. The proposed approach addresses both overall and local responses of unreinforced masonry buildings subjected to excavation-induced settlement along with self-weight by introducing both direct FEM results called conventional parameters and indirect FEM results used for building damage assessment called validation performance. In the three building facades tested, discrepancies of maximum relative errors were no more than 1.1% of building dimensions and that of both relative stiffness and opening ratio limited to within 4%. The geometric discrepancies impacted the applied loading, particularly as building width controlled the location of the imposed displacements due to excavation. The examples showed the various effects of discrepant building geometries on structural response and the importance of considering both global and local parameters in any validation procedure.

Acknowledgments

This work was made possible through the generous funding of Science Foundation Ireland (SFI/PICA/I850).

Appendix A

Nodal displacement comparisons allow structural health evaluation by the movement magnitude and direction of a structural component to a pre-defined limit. Nodal movements determined from displacement gauges from experimental tests can easily be identified and tracked within the computational mesh.

Nodal stress/strain comparisons enable structural safety determination by examining the internal load acting on a unit area or deformation over its unit length, compared to the known (or anticipated) material strength and strain limits. Experimentally, strain gauges measure deformations with respect to the Modulus of Elasticity at specific locations from which the stress can then be derived. In numerical models, these values can be obtained directly from a FEM solution. However, the measured strain is not often used, because of the unpredictable maximum strain level in a structure, the highly localized nature of the approach, and the limitations of strain range measurement (particularly during large deformations).

Load versus displacement comparisons show the evolution of deformation during loading. This item is used to validate the proposed method in predicting a structure's overall deformation response. Similar to nodal displacement, both load and displacements are easily established based on values of a load cell(s) versus a displacement gauge(s) during experimentation or the input load versus the output displacements in a computational model.

Cracking pattern comparisons document the propagation of separation patterns of building components versus loading/displacement, which can explicitly display a structure's failure mechanism. While cracking propagation can be visually observed to confirm that the failure mechanism is consistent with the predicted one, cracking parameters (crack width and length) cannot readily be measured during the load-

ing/displacement of a structure. Those values can only be obtained at the end of each load step.

Ultimate strength comparisons consider the maximum loading born by a structure, which is often used to determine the accuracy of the capacity estimation of a proposed method. The ultimate strength can be obtained based on a load-displacement relationship established during experimental or numerical testing.

Computational cost comparisons involve computer recourses and running time, and arguably the extent of human intervention needed when comparing different modeling strategies. This item helps to evaluate the balance between accuracy and analysis costs.

References

[1] Cai, H. and Rasdorf, W., "Modeling road centrelines and predicting lengths in 3D using LiDAR point cloud and planimetric road centreline data," *Computer-Aided Civil and Infrastructure Engineering*, Vol. 23 (3), 2008, pp. 157-173,

[2] Laefer, D. F. and Pradhan, A. R., "Evacuation route selection based on tree-based hazards using LiDAR and GIS," *ASCE Journal of Transportation Engineering*, Vol. 132 (4), 2006, pp. 312-320,

[3] Gordon, S., Lichti, D., Stewart, M. and Franke, J., "Measurement of Structural Deformation using Terrestrial Laser Scanners," *1st FIG International Symposium on Engineering Surveys for Construction Works and Structural Engineering*, Nottingham, United Kingdom, 28 June – 1 July, 2004, pp. 16.

[4] Laefer, D. F., Hinks, T. and Carr, H., "New possibilities for damage prediction from tunnel subsidence using aerial LiDAR data," *ISSMGE, Geotechnical Challenges in Megacities*, Moscow, Russia, 7-10 June, 2010.

[5] Guarnieri, A., Pirotti, F., Pontin, M. and Vettore, A., "Combined 3D surveying Techniques for Structural Analysis Applications," *3D-ARCH 2005: Virtual Reconstruction and Visualization of Complex Architectures* Vol. XXXVI-5/W17, Mestre-Venice, Italy, 22-24 August, 2005, pp. 6.

[6] Independent, 2006, Port Tunnel compo payout, http://www.independent.ie/opinion/letters/port-tunnel-compo-payout-75149.html, Accessed date: 10 Dec, 2011.

[7] Post, R., 2009, Subway Tunnel Collapse in Cologne Germany, http://www.geoprac.net/geonews-mainmenu-63/38-failures/456-subway-tunnel-collapse-in-cologne-germany, Accessed date: 10th Dec, 2011.

[8] Laefer, D. F., Truong-Hong, L. and Fitzgerald, M., "Processing of Terrestrial Laser Scanning Point Cloud Data for Computational Modelling of Building Facades," *Recent Patents on Computer Science*, Vol. 4 (1), 2011, pp. 16-29,

[9] Wehr, A. and Lohr, U., "Airborne laser scanning-an introduction and overview," *ISPRS Journal of Photogrammetry and Remote Sensing*, Vol. 25 (1-2), 1999, pp. 68-92,

[10] Wenisch, P., Treeck, C. V., Borrmann, A., Rank, E. and Wenisch, O., "Computational steering on distributed systems: Indoor comfort simulations as a case study of interactive CFD on supercomputers," *International Journal of Parallel, Emergent and Distributed Systems*, Vol. 22 (4), 2007, pp. 275-291, 10.1080/17445760601122183.

[11] ASME, *PTC 60 / V&V 10 Guide for Verification and Validation in Computational Solid Mechanics*, American Society of Mechanical Engineers, NewYork, 2006, p. 36

[12] Guenfoud, S., Bosakov, S. V. and Laefer, D. F., "Dynamic analysis of a beam resting on an elastic half-space with inertial properties," *Soil Dynamics and Earthquake Engineering*, Vol. 29 (8), 2009, pp. 1198-1027,

[13] Lourenco, P. B., Rots, J. G. and Blaauwendraad, J., "Two approaches for the analysis of masonry structures: micro and macro modeling," *Heron*, Vol. 40 (4), 1995, pp. 313-340,

[14] Chaimoon, K. and Attard, M. M., "Modeling of unreinforced masonry walls under shear and compression," *Engineering Structures*, Vol. 29 (9), 2007, pp. 2056-2068,

[15] Truong-Hong, L. and Laefer, D., "Micro vs. Macro Models for Predicting Building Damage Underground Movements," *International Conference on Computational Solid Mechanics -CSM2008*, Ho Chi Minh City, Vietnam, 27-30 November, 2008, pp. 259-268.

[16] Roca, P., Molins, C. and Marí, A. R., "Strength Capacity of Masonry Wall Structures by the Equivalent Frame Method," *Journal of Structural Engineering, ASCE*, Vol. 131 (10), 2005, pp. 1601-1610,

[17] Zucchini, A. and Lourenço, P. B., "A micro-mechanical homogenisation model for masonry: Application to shear walls," *International Journal of Solids and Structures*, Vol. 46 (3), 2009, pp. 871-886,

[18] Orduña, A. and Lourenço, P. B., "Three-dimensional limit analysis of rigid blocks assemblages. Part II: Load-path following solution procedure and validation," *International Journal of Solids and Structures*, Vol. 42 (18-19), 2005, pp. 5161-5180,

[19] Kappos, A. J., Penelis, G. G. and Drakopoulos, C. G., "Evaluation of Simplified Models for Lateral Load Analysis of Unreinforced Masonry Buildings," *ASCE Journal of Structural Engineering*, Vol. 128 (7), 2002, pp. 890-897,

[20] Sincraian, G. E. and Azevedo, J. J., "Numerical simulation of the seismic behaviour of stone and brick masonry structures using the discrete element method," *11th European Conference on Earthquake Engineering*, Paris la Défense, France, 6-11 September, 1998, pp. CD-ROM.

[21] Mohebkhah, A., Tasnimi, A. A. and Moghadam, H. A., "Nonlinear analysis of masonry-infilled steel frames with openings using discrete element method," *Journal of Constructional Steel Research*, Vol. 64, 2008, pp. 1463-1472,

[22] Mo, T.-B., Shi, G.-B., Wang, Q.-L. and Yi, W.-Z., "The behavior and strength of brick and reinforced concrete composite wall beams with door opening," *The proceeding of Eighth International Brick and Block Masonry*, Vol. 1, Trinity College Dublin, Republic of Ireland, 19-21 September, 1988, pp. 384-394.

[23] Asteris, P. G., "Lateral Stiffness of Brick Masonry Infilled Plane Frames," *ASCE Journal of Structural Engineering*, Vol. 129 (8), 2003, pp. 1071-1079,

[24] Pickhaver, J. A., Numerical Modelling of Building Response to Tunnelling, PhD thesis, Balliol College, University of Oxford, 2006.

[25] Laefer, D. F., Hinks, T., Carr, H. and Truong-Hong, L., "New Advances in Automated Urban Model Population through Aerial Laser Scanning," *Recent Patents in Engineering*, Vol. 5 (3), 2011, pp. 196-208,

[26] Truong-Hong, L. and Laefer, D., "Impact of Modeling Architectural Detailing for Predicting Unreinforced Masonry Response to Subsidence," *Automation in Construction*, Vol., 2012, pp. Accepted,

[27] Liu, G., Houlsby, G. T. and Augarde, C. E., "2-dimensional analysis of settlement damage to masonry buildings caused by tunnelling," *The structural Engineer*, Vol. 79 (1), 2000, pp. 19-25,

[28] Mair, R. J. and Taylor, R. N., *Settlement predictions for Neptune, Murdoch and Clegg Houses and adjacent masonry walls*, in: S.J.R. Burland J.B., and Jardine F.M. (Ed.), Building Response to Tunnelling: Case Studies from Construction of the Jubilee Line Extension, London, Vol. 1: Projects and Methods, CIRIA and Thomas Telford, 2001, pp. 217-228.

[29] Boonpichetvong, M. and Rots, J. G., "Settlement damage of masonry building in soft-ground tunnelling," *Processing the third DIANA World Conference: Finite Elements in Civil Engineering Applications*, Tokyo, Japan, 9-11 October, 2002, pp. 285-293.

[30] Skinner, H., *Issue 475 of Digest Series: Tilt of low-rise buildings with particular reference to progressive foundation movement*, BRE Electronic Publications, 2003, p. 8

[31] Burland, J. B., "Assessment of Risk Damage to Buildings due to Tunneling and Excavation," *1st International Conference on Earthquake Geotechnical Engineering. Invited special lecturer to IS-Tokyo*, Tokyo, 1995, pp. 14.

[32] Bažant, Z. P. and Planas, J., *Fracture and Size Effect in Concrete and Other Quasibrittle Materials*, CRC Press, 1997, p. 640

[33] Bazant, Z. P. and Cedolin, L., "Finite Element Modeling of Crack Band Propagation," *ASCE Journal of Structural Engineering*, Vol. 109, 1983, pp. 69-92,

[34] Rots, J. G., Computational Modeling of Concrete Fracture, PhD thesis, Civil Engineering and Geosciences, TUDelft, 1988.

[35] Oliver, J., "A Consistent Characteristic Length for Smeared Cracking Models," *International Journal for Numerical Methods in Engineering*, Vol. 28 (2), 1989, pp. 461-474,

[36] Scotta, R., Vitaliani, R., Saetta, A., Oñate, E. and Hanganu, A., "A Scalar Damage Model with A Shear Retention Factor for The Analysis of Reinforced Concrete Structures: Theory and Validation," *Computers & Structures*, Vol. 79 (7), 2001, pp. 737-755,

[37] ANSYS Academic Research Release 13.0, Help System, Theory Reference for ANSYS and ANSYS Workbench.

[38] Skempton, A. W. and MacDonald, D. H., "The Allowable Settlements of Buildings," *ICE Proceedings: Engineering Divisions*, Vol. 5 (6), 1956, pp. 727-784,

[39] Burland, J. B. and Wroth, C. P., "Settlements on Buildings and Associated Damage.," *The British Geotechnical Society's Conference on the Settlement of Structures*, Vol., 1974, pp. 611–654,

[40] Boscardin, M. D. and Cording, E. J., "Building Response to Excavation-Induced Settlement," *ASCE Journal of Geotechnical and Geoenvironmental Engineering*, Vol. 115 (1), 1989, pp. 1-21,

[41] Boone, S. J., "Ground-Movement-Related Building Damage," *ASCE Journal of Geotechnical and Geoenvironmental Engineering*, Vol. 122 (11), 1996, pp. 886-896,

[42] Cording, E. J., Long, J. H., Son, M. and Laefer, D. F., "Modelling and Analysis of Excavation-Induced Building Distortion and Damage Using a Strain-Based Damage Criterion," *Proceeding of International Conference for Responses of Buildings to Excavation-Induced Ground Movements*, London, 17-18 July, 2001, pp. CD ROM.

[43] Oberkampf, W. and Barone, M., "Measures of Agreement between Computation and Experiment: Validation Metrics," *Journal of Computational Physics*, Vol. 217 (1), 2006, pp. 5-36,

[44] Devore, J. L., *Probability and Statistics for Engineering and the Sciences*, 5th ed., Duxbury, 1999, p. 750

[45] Trimble, 2005, Trimble G200, http://www.trimble.com, Accessed date: November 25, 2011.

[46] Trimble, 2010, RealWorks Survey, http://www.trimble.com/realworks.shtml, Accessed date: November 25, 2011.

[47] Truong-Hong, L., Laefer, D. F., Hinks, T. and Carr, H., "Flying Voxel Method with Delaunay Triangulation Criterion for Façade/Feature Detection for Computation," *ASCE Journal of Computing in Civil Engineering*, Vol. 26 (6), 2012, pp. 691–707,

[48] Truong-Hong, L., Automatic Generation of Solid Models of Building Façades from LiDAR Data for Computational Modelling, PhD, School of Architecture, Landscape and Civil Engineering, University College Dublin, 2011.

[49] Lourenço, P. B., Computational Strategies for Masonry Structures., PhD thesis, Civil Engineering Department, Delft University of Technology, 1996.

[50] William, K. J. and Warnke, E. D., "Constitutive Model for The Triaxial Behaviour of Concrete," *Proceedings of International Association for Bridge and Structural Engineering*, Vol. III, Bergamo, Italy, 1975, pp. 1-30.

[51] Drucker, D. C. and Prager, W., "Soil Mechanics and Plastic Analysis for Limit Design," *Quarterly of Applied Mathematics*, Vol. 10 (2), 1952, pp. 157-165,

[52] Pluijm, R. V. d., "Shear Behavior of Bed Joints," *Proceeding of 6th North American Masonry Conference*, Philadelphia, Pennsylvania, USA, 3-6 June, 1990, pp. 125-136.

[53] Lourenço, P. B., Barros, J. O. and Oliveira, J. T., "Shear Testing of Stack Bonded Masonry," *Construction and Building Materials*, Vol. 18 (2), 2004, pp. 125-132,

[54] Laefer, D., F., Prediction and Assessment of Ground Movement and Building Damage Induce by Adjacent Excavation, PhD, Department of Civil and Environment Engineering, University of Illinois at Urbana-Champaign, 2001.

[55] Shah, C., "Mesh Discretization Error and Criteria for Accuracy of Finite Element Solutions," *Ansys Users Conference*, Pittsburgh, PA, 28 March, 2002, pp. 12.